Neurobiology of Disease 156 (2021) 105409

Contents lists available at ScienceDirect

Neurobiology of Disease

journal homepage: www.elsevier.com/locate/ynbdi

Mitochondrial oxidant stress mediates methamphetamine neurotoxicity in substantia nigra dopaminergic neurons

Steven M. Graves [a], Sarah E. Schwarzschild [b], Rex A. Tai [b], Yu Chen [b], D. James Surmeier [b,*]

[a] Department of Pharmacology, University of Minnesota, Minneapolis, MN 55455, United States of America
[b] Department of Physiology, Feinberg School of Medicine, Northwestern University, Chicago, IL 60611, United States of America

ARTICLE INFO

Keywords:
Methamphetamine
Mitochondrial stress
Monoamine oxidase
Dopamine
Parkinson's disease
Degeneration

ABSTRACT

Methamphetamine abuse is associated with an increased risk of developing Parkinson's disease (PD). Recently, it was found that methamphetamine increases mitochondrial oxidant stress in substantia nigra pars compacta (SNc) dopaminergic neurons by releasing vesicular dopamine (DA) and stimulating mitochondrially-anchored monoamine oxidase (MAO). As mitochondrial oxidant stress is widely thought to be a driver of SNc degeneration in PD, these observations provide a potential explanation for the epidemiological linkage. To test this hypothesis, mice were administered methamphetamine (5 mg/kg) for 28 consecutive days with or without pretreatment with an irreversible MAO inhibitor. Chronic methamphetamine administration resulted in the degeneration of SNc dopaminergic neurons and this insult was blocked by pretreatment with a MAO inhibitor – confirming the linkage between methamphetamine, MAO and SNc degeneration. To determine if shorter bouts of consumption were as damaging, mice were given methamphetamine for two weeks and then studied. Methamphetamine treatment elevated both axonal and somatic mitochondrial oxidant stress in SNc dopaminergic neurons, was associated with a modest but significant increase in firing frequency, and caused degeneration after drug cessation. While axonal stress was sensitive to MAO inhibition, somatic stress was sensitive to Cav1 Ca^{2+} channel inhibition. Inhibiting either MAO or Cav1 Ca^{2+} channels after methamphetamine treatment attenuated subsequent SNc degeneration. Our results not only establish a mechanistic link between methamphetamine abuse and PD, they point to pharmacological strategies that could lessen PD risk for patients with a methamphetamine use disorder.

1. Introduction

Drug addiction is a debilitating disease that causes enormous personal and socioeconomic harm. Recently, the number of people suffering from a methamphetamine (MA) use disorder has increased significantly (NSDUH, 2018; Winkelman et al., 2018). This trend is particularly concerning given that MA has the potential to cause lasting brain damage. Post-mortem analysis from human MA abusers reveals that striatal levels of dopamine (DA), DA transporter (DAT), and the DA synthetic enzyme tyrosine hydroxylase are decreased (Kish et al., 2009; Kitamura et al., 2007; Moszczynska et al., 2004; Wilson et al., 1996). Consistent with these reports, imaging of MA abusers has revealed a loss of striatal DAT and vesicular monoamine transporter 2 (VMAT2) binding, as well as morphological abnormalities indicative of damage to the substantia nigra (Johanson et al., 2006; McCann et al., 2008; McCann et al., 1998; Rumpf et al., 2017; Sekine et al., 2001; Todd et al., 2013; Todd et al., 2016; Volkow et al., 2001a; Volkow et al., 2001b). In concert with these findings, epidemiological studies have uncovered a linkage between MA abuse and the risk of developing Parkinson's disease (PD) (Callaghan et al., 2010; Callaghan et al., 2012; Curtin et al., 2015). This connection is not entirely surprising as the cardinal motor symptoms of PD result from the degeneration of substantia nigra pars compacta (SNc) dopamine neurons that innervate the striatum (Surmeier et al., 2017b).

Although the phenomenology is clear, the mechanisms mediating MA-induced degeneration of dopaminergic neurons remains to be fully elucidated. MA has two key targets: DAT which moves DA from the extracellular space to the cytosol and VMAT2 which pumps cytosolic DA into synaptic vesicles. By disrupting VMAT2 function, MA increases the

Abbreviations: methamphetamine, MA; monoamine oxidase, MAO; substantia nigra pars compacta, SNc; tyrosine hydroxylase, TH; dopamine, DA; dopamine transporter, DAT; vesicular monoamine transporter 2, VMAT2.

* Corresponding author at: Department of Physiology, Feinberg School of Medicine, Northwestern University, 303 E. Chicago Ave., Chicago, IL 60611, USA.
E-mail address: j-surmeier@northwestern.edu (D.J. Surmeier).

https://doi.org/10.1016/j.nbd.2021.105409
Received 20 February 2021; Received in revised form 12 May 2021; Accepted 28 May 2021
Available online 31 May 2021

cytosolic DA concentration (Freyberg et al., 2016; Sulzer et al., 2005). Historically, it has been thought that cytosolic DA is damaging either because it rapidly auto-oxidizes into reactive quinones or that its metabolism by monoamine oxidase (MAO) increases cytosolic H_2O_2 and oxidant stress (Edmondson, 2014; Edmondson et al., 2009; Sulzer and Zecca, 2000). However, using a genetically encoded redox sensor, it was shown that MA has little or no detectable effect on cytosolic redox status in dopaminergic neurons; rather, MA significantly increases mitochondrial stress (Graves et al., 2020). This stress was a reflection of a mechanism that supports the bioenergetic demands associated with dopamine release and uptake. Mitochondrially tethered MAO metabolizes cytosolic DA and transfers the electron generated to the electron transport chain, where it helps support the proton gradient used to drive ATP synthesis (Graves et al., 2020). When this mechanism is excessively stimulated by MA release of vesicular DA, oxidant stress is created in axons where DA is stored and released. The consequences of repeated 'over-stimulation' of this pathway by chronic MA use has not been investigated.

Another source of mitochondrial stress in SNc dopaminergic neurons arises from somatodendritic Ca^{2+} influx through Cav1 Ca^{2+} channels during pacemaking (Chan et al., 2007; Guzman et al., 2018; Guzman et al., 2010; Surmeier et al., 2017a). It is unclear whether chronic MA use has any lasting effects on somatodendritic excitability or mitochondrial stress that might contribute to degeneration.

The present study was designed to address these knowledge gaps and to identify druggable targets that might mitigate the damaging effects of MA. Using a combination of optical, electrophysiological, and immunohistochemical approaches, it was confirmed that chronic MA administration to mice results in SNc degeneration. This degeneration was mitigated by inhibition of type B MAO (MAO-B). A shorter bout of MA administration led to a delayed degeneration that also was attenuated by MAO-B inhibition after cessation of MA administration. Unexpectedly, MA treatment also accelerated somatodendritic pacemaking, resulting in a local elevation in mitochondrial stress. This activity-induced stress also contributed to the delayed degeneration as Cav1 channel inhibition diminished loss of SNc dopaminergic neurons after MA administration.

2. Methods

2.1. Experimental subjects

Male mice expressing the redox sensitive roGFP probe targeting the mitochondrial matrix under the tyrosine hydroxylase regulatory element (Graves et al., 2020; Guzman et al., 2010), tdTomato under the dopamine transporter regulatory element (DAT-cre X Ai14-tdTomato) (Galtieri et al., 2017), eGFP under the *Drd2* regulatory element (Chan et al., 2012), and wild-type mice (C57/Bl6) were bred in-house and used throughout with approval from the Northwestern University Animal Care and Use Committee and in accordance with the National Institutes of Health Guide for the Care and Use of Laboratory Animals. Transgenic subjects were hemizygous for transgenes. Animals were group housed with food and water provided *ad libitum* on a 12-h light/dark cycle. All experimental mice were sacrificed between 8 and 12 weeks of age. Only male mice were used in the experiments for two reasons. First, because the incidence of PD is lower in females (Cerri et al., 2019), sex is likely to affect the response to challenges that may cause PD. Second, preliminary work in our lab suggests that indeed basal mitochondrial oxidant stress in dopaminergic neurons of female mice is lower than that of males. Powering the study to adequately resolve sex differences in the response to MA would have required that the sample sizes be doubled, which was not possible for budgetary reasons. The role of sex in the response to MA treatment should be rigorously pursued in a future study.

2.2. Surgical procedures

Subjects were anesthetized in an induction chamber using a low-flow isoflurane precision vaporizer (Kent Scientific) and placed in a stereotaxic frame (David Kopf Instruments) with a Cunningham adaptor (Harvard Apparatus) to maintain isoflurane anesthesia throughout surgery with periodic toe-pinches to verify anesthetic depth. The skull was exposed, a small hole drilled, and 350 nl of AAV9-TH-cytosolic roGFP delivered *via* a glass micropipette (Drummond Scientific Company) pulled on a Sutter P-97 puller. The SNc was targeted using the following coordinates: AP: -3.05, ML: 1.20, and DV -4.30. Experiments using *ex vivo* brain slices from animals with stereotaxic delivery of AAV were performed >10 days post-op. In experiments to assess the effect of isradipine administration after cessation of MA treatment isradipine was delivered by subcutaneous osmotic minipumps (Alzet; model 2002). Minipumps were loaded with isradipine dissolved in 50% DMSO/15% PEG300/double-distilled water at a concentration to achieve 3 mg/kg/day dosing (Guzman et al., 2018; Ilijic et al., 2011). Pumps were placed in 0.9% saline at 37 °C overnight prior to implantation. Pumps were implanted subcutaneously as previously described (Guzman et al., 2018; Ilijic et al., 2011) and per manufacturers guidelines; at the time of sacrifice pumps were removed and visually inspected to verify that drug was delivered.

2.3. Brain slice preparation, electrophysiology, and Ca^{2+} imaging

Mice were anesthetized with ketamine (50 mg/kg)/xylazine (4.5 mg/kg; i.p.) and transcardially perfused with ice cold modified artificial cerebrospinal fluid (aCSF) containing 124.0 mM NaCl, 3.0 mM KCl, 1.0 mM $CaCl_2$, 2.0 mM $MgCl_2$, 26 mM $NaHCO_3$, 1.0 mM NaH_2PO_4, and 16.66 mM glucose. The brain was rapidly removed and saggital or coronal brain slices entailing the dorsolateral striatum (275 μm thick) or the SNc (220 μm thick) sectioned using a vibratome (VT1200S Leica Microsystems). Slices were transferred to a holding chamber with normal aCSF containing 124.0 mM NaCl, 3.0 mM KCl, 2.0 mM $CaCl_2$, 1.0 mM $MgCl_2$, 26 mM $NaHCO_3$, 1.0 mM NaH_2PO_4, and 16.66 mM glucose and allowed a minimum of 30 min to recover prior to experiments. Solutions were pH 7.4 and 310–320 mOsm with 95% O_2/5% CO_2 continuously bubbled. For experiments using perforated patch clamp techniques pipettes were filled with internal solution containing 126 mM KMeSO4 methylsulfate, 14 mM KCl, 10 mM HEPES, 1.0 mM EGTA, 0.5 mM $CaCl_2$, and 3.0 mM $MgCl_2$; electrical access was achieved using gramicidin D (~20 μg/ml) dissolved in the same internal solution. Pipettes were front filled with internal solution lacking gramicidin and then backfilled with the internal solution containing gramicidin (Estep et al., 2016). Perforated patch techniques were used to examine pacemaking frequency because this technique provides access to the transmembrane potential without the confound of rundown. To facilitate identification of nigral dopaminergic neurons experiments were conducted in tissue from D_2-eGFP mice. To record Ca^{2+} oscillations tissue from wild-type subjects was used with whole-cell patch clamp techniques. Internal solution for whole-cell recordings consisted of 135 mM $KMeSO_4$, 5.0 mM KCl, 10 mM HEPES, 10.0 mM phosphocreatine-di (tris), 2.0 mM ATP—Mg, 0.5 mM GTP-Na and 200 μM Fura-2. Electrophysiological recordings were performed on visually identified SNc neurons using an Olympus 60/0.9NA lens in a submersion-style recording chamber mounted on an Olympus BX51 upright, fixed stage microscope using a multiclamp 700B amplifier controlled by PrairieView software. Two-photon laser scanning microscopy was used to record Fura-2 fluorescence as previously described (Guzman et al., 2018). In brief, Ca^{2+} imaging was performed using a Chameleon Ultra II laser. Fluorescent signal was acquired using 780 nm excitation with laser power attenuation *via* Pockels cell electrooptic modulators (Conoptics) controlled by PrairieView software (Ultima, Bruker Technologies) with fluorescence emission collected by photomultiplier tubes (PMTs). Fluorescence measurements were acquired at proximal (<80 μm from the soma) and distal (<80 μm from the soma) dendritic segments; signal was calibrated by holding the membrane potential below −60 mV to minimize Ca^{2+} and obtain the f_{max} value (Guzman et al., 2018). All

internal pipette solutions were pH 7.25–7.3 and ~280 mOsm.

2.4. Oxidant stress measurements

Mitochondrial and cytosolic oxidant stress was measured using the redox sensitive roGFP probe targeted to the cytosol or mitochondrial matrix (Graves et al., 2020; Guzman et al., 2010). Slices were transferred to a recording chamber with normal aCSF at 32–34 °C continuously perfused. Measurement and analyses are consistent with prior studies (Graves et al., 2020). In brief, fluorescence was measured using an Ultima Laser Scanning Microscope system (Bruker) with an Olympus 60/0.9NA lens and PrairieView software. An excitation wavelength of 920 nm was applied using a two-photon laser (Chameleon Ultra II, Coherent Inc.) to excite roGFP. A *t*-series of roGFP fluorescence was obtained with 60 frames acquired over ~20 s with 0.195 μm × 0.195 μm pixels and 10–12 μsec dwell time. The probe was calibrated by obtaining the dynamic range; this was accomplished by acquiring additional *t*-series with bath perfusion of 2 mM dithiothreitol, a reducing agent, and 200 μM aldrithiol, an oxidizing agent, to determine the maximal and minimal fluorescence intensity as previously described (Graves et al., 2020). Test measurements were calculated as relative oxidation, data normalized to controls, and presented as % control.

2.5. Immunohistochemistry, stereological, and densitometric analysis

Mice were anesthetized with a mixture of ketamine (50 mg/kg)/xylazine (4.5 mg/kg) and transcardially perfused with 4% paraformaldehyde, post-fixed overnight and cryoprotected in 30% sucrose/phosphate buffered saline (PBS) at 4 °C until use. Immunohistochemical and stereological procedures were performed as previously described (Ilijic et al., 2011). Serial coronal sections were collected throughout the midbrain to stain for tyrosine hydroxylase using the anti-tyrosine hydroxylase polyclonal antibody (Millipore) 1:2000 followed by goat anti-rabbit IgG biotin conjugated antibody (Millipore) 1:500 with normal goat serum blocking solution was used; after antibody incubation and rinsing with PBS, sections were incubated with ABC Elite Kit (Vector) and processed for diaminobenzidine reaction. Slices were mounted on slides, dehydrated in ascending alcohol concentrations and mounted with DPX mountant (Sigma). The number of tyrosine hydroxylase positive (TH^+) cells in the SNc were stereologically counted using the optical fractionator protocol as previously described (Ilijic et al., 2011), Slices from DAT-Cre X Ai14 mice expressing tdTomato in dopaminergic neurons were mounted on slides, allowed to dry, and mounted with Prolong Gold antifade mountant (Invitrogen). The number of tdTomato expressing neurons in the SNc were also stereologically counted using the optical fractionator protocol. An Olympus BX41 microscope with motorized stage (Applied Scientific Instrumentation) and computerized stereology software (Stereologer) was used for all stereological analyses. The SNc was delineated in each animal in every other section and cells counted using a 40×/0.65NA Olympus lens. Optical density of axonal fibers expressing tdTomato from DAT-Cre X Ai14 mice in the striatum was determined from eight coronal sections from each animal encompassing the rostral-caudal extension of the striatum (Ilijic et al., 2011).

2.6. Real-time PCR

Brains were removed and the SNc from mice treated with saline ($n = 6$ mice) or MA ($n = 5$ mice) was dissected under a light microscope using a 10× lens. Total mRNA was isolated with RNeasy Micro Kit (Qiagen, Inc.) and DNA contamination was removed with an on-column DNaseI (Qiagen, Inc.) treatment. About 0.2–0.5 μg of total mRNA of each sample was reverse transcribed into first strand cDNA using SuperScript VILO cDNA synthesis kit (Invitrogen by Thermo Fisher Scientific). Quantitative real-time PCR was performed using an ABI StepOnePlus Real Time PCR system with TaqMan Gene Expression Assays (Applied Biosystems by Thermo Fisher Scientific). Transcript gene probes used for Real-Time PCR were designed by ABI TaqMan Gene Expression Assays. GAPDH Assay ID*were Mm99999915_g1, VMAT2 Assay ID* were Mm00553058_m1, CacnaD1 Assay ID* were Mm01209927_g1. The relative abundance of transcripts was assessed by TaqMan quantitative PCR in triplicate for each mouse subject. The final expression levels were shown as ΔCt values. The cycling protocol consisted on 50 °C for 2 min, then 95 °C for 10 min followed by 40 cycles at 95 °C for 15 s, 60 °C for 1 min (TaqMan Reagents Standard run). The CT value in each group of samples were characterized by their median values. GAPDH were used as endogenous control and wild type control sample1 used as reference sample. ABI StepOnePlus software V2.3 perform comparative CT(ΔΔCt) was used to analyze data; Relative Quantitation results were presented as fold changes relative to the median of wild type controls (*i.e.* saline treated mice). We used Microsoft® Excel to open the exported Ct file from an ABI StepOnePlus PCR analysis system and then to transform data into a tab delimited text file for SAS processing.

2.7. Drug treatment

In vivo drug treatments included repeated saline, (+)-methamphetamine (MA), or rasagiline all of which were administered i.p.; *in vivo* isradipine (3 mg/kg/day) was administered *via* implantation of a subcutaneous osmotic minipump (Alzet) consistent with prior studies (Guzman et al., 2018; Ilijic et al., 2011). To determine the effects of repeated MA, mice were treated daily for 28 or 14 consecutive days with MA (5 mg/kg; Sigma-Aldrich) and mice sacrificed on the 28th day of MA administration (within 24 h of the last injection) or 1, 7, or 14 days after cessation of MA treatment. To determine whether MAO inhibition could prevent MA-induced effects, rasagiline (1 mg/kg) was administered as a 30-min pretreatment prior to each MA injection in the 28-day treatment paradigm or daily after cessation of MA treatment. Drug application in *ex vivo* brain slices was performed *via* perfusion in aCSF.

2.8. Statistical analysis

Data were analyzed in Prism (GraphPad Software La Jolla, CA) using non-parametric statistics and presented as box-and-whisker plots depicting median, quartiles, and range. Mann-Whitney (two-tailed) and Kruskal-Wallis with Dunns post-hoc analyses were used throughout. PCR data was analyzed using parametric *t*-tests. All data have been normalized to respective controls and presented as a % control; $\alpha = 0.05$. 'Control' groups in each figure were derived from separate groups of mice and at no time were data used for multiple analyses.

3. Results

3.1. Chronic methamphetamine administration caused MAO-dependent SNc degeneration

Patients suffering from MA use disorders repeatedly consume moderate to large quantities for months to years (Boileau et al., 2016; Boileau et al., 2008; Johanson et al., 2006; McCann et al., 2008; McCann et al., 1998; Moszczynska et al., 2004; Rumpf et al., 2017; Sekine et al., 2001; Sekine et al., 2006; Volkow et al., 2001a; Volkow et al., 2001b; Wilson et al., 1996). To determine the consequence of chronic MA consumption on SNc dopaminergic neurons, mice were treated with MA (5 mg/kg; i.p) or saline for 28 consecutive days and sacrificed on day 28. Paraformaldehyde fixed brain slices were stained for tyrosine hydroxylase (TH) to identify dopaminergic neurons and the number of SNc dopaminergic neurons stereologically counted (Ilijic et al., 2011). Chronic (28 day) *in vivo* MA administration resulted in an approximate 30% loss of TH^+ SNc dopaminergic neurons **(**Fig. 1A**)**.

MA disrupts the sequestration of cytosolic DA by VMAT2, thereby increasing concentrations of cytosolic DA (Freyberg et al., 2016; Sulzer et al., 2005). The interaction between MA and VMAT2 known to be a key factor mediating the deleterious effects of MA with knockout or

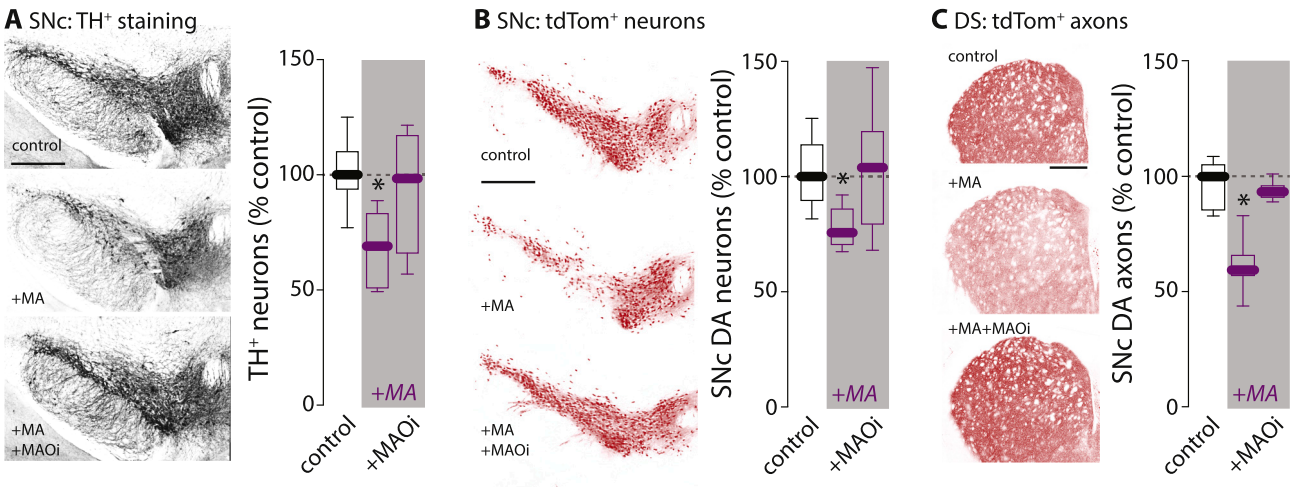

Fig. 1. Chronic 28-day *in vivo* methamphetamine administration was neurotoxic to substantia nigra pars compacta dopamine neurons. A, Sample images depicting chronic 28-day methamphetamine (+MA; 5 mg/kg i.p.)-induced loss of tyrosine hydroxylase expressing (TH^+) neurons (left) in the substantia nigra pars compacta (SNc) which was prevented by monoamine oxidase inhibition (1 mg/kg rasagiline pretreatment; +MAOi). Stereological quantification indicates a loss of TH^+ neurons after +MA that was prevented with +MAOi (right); control $n = 6$ (median TH^+ cells = 11,342), +MA $n = 7$ (median TH^+ cells = 7829), and + MAOi $n = 4$ mice (median TH^+ cells = 11,168); Kruskal-Wallis test with Dunn's *post-hoc*. B, Sample images depicting chronic 28-day methamphetamine (+MA; 5 mg/kg i.p.)-induced loss of fluorescently labeled neurons from Dat-Cre X Ai14 mice (left) which was prevented by monoamine oxidase inhibition (1 mg/kg rasagiline 30 min pretreatment; +MAOi). Stereological quantification indicates a loss of SNc neurons after +MA that was prevented with +MAOi (right); control n = 7 (median Tom^+ cells = 15,923, +MA $n = 7$ (median Tom^+ cells = 12,051), and + MAOi n = 7 (median Tom^+ cells = 16,531) mice (Kruskal-Wallis test with Dunn's *post-hoc)*. C, Sample images depicting chronic 28-day methamphetamine (+MA; 5 mg/kg i.p.)-induced loss of fluorescently labeled axons in the striatum from Dat-Cre X Ai14 mice (left) which was prevented by monoamine oxidase inhibition (1 mg/kg rasagiline 30 min pretreatment; +MAOi; changes quantified by optical density measurements (right); control $n = 8$, +MA $n = 8$, and + MAOi $n = 8$ mice (Kruskal-Wallis with Dunn's *post-hoc*). Scale bars denote 500 μm; $^*p < 0.05$ compared to control.

downregulation of VMAT2 exacerbating the damaging effects of MA (Fumagalli et al., 1999; Guillot et al., 2008b; Larsen et al., 2002) whereas increasing VMAT2 affords resistance (Guillot et al., 2008a; Lohr et al., 2015). Once released from vesicles into the cytosol, cytosolic DA increases mitochondrial oxidant stress by stimulating the activity of MAO anchored to the outer membrane of mitochondria in axons (Graves et al., 2020). To determine whether MAO inhibition could attenuate MA-induced degeneration of SNc dopaminergic neurons, mice were chronically treated with MA (as described above) but were given the irreversible MAO-B inhibitor rasagiline (1 mg/kg; i.p.) 30 min prior to MA. Pretreatment with rasagiline prevented chronic MA-induced loss of TH^+ SNc dopaminergic neurons (Fig. 1A).

To confirm that chronic MA treatment resulted in neuronal loss and not phenotypic suppression, experiments were repeated in DAT-Cre mice crossed into the Ai14 reporter line having a floxed tdTomato reporter construct in the Gt(ROSA)26Sor locus. Chronic MA decreased the number of tdTomato expressing neurons in the SNc and axons in the striatum, consistent with the proposition that MA treatment induced frank neurodegeneration (Fig. 1B, C). Again, pretreatment with the MAO inhibitor rasagiline prevented loss of tdTomato expression (Fig. 1B, C). Taken together these data indicate that chronic MA treatment induces degeneration of SNc dopaminergic neurons through a MAO-B dependent mechanism.

3.2. MA induced a MAO-dependent delayed degeneration

To determine whether chronic (28 day) MA administration was necessary for degeneration, subjects were treated with MA (5 mg/kg; i.p.) for 14 consecutive days and sacrificed 1, 7, or 14 days later. Fourteen days after stopping MA administration, but not at 1 or 7 days, the number of TH^+ SNc neurons had declined (Fig. 2).

To better understand what was causing the change, mitochondrial and cytosolic oxidant stress were examined in axonal and somatic compartments of SNc dopaminergic neurons in *ex vivo* brain slices from mice after the 14 day MA treatment protocol. Surprisingly,

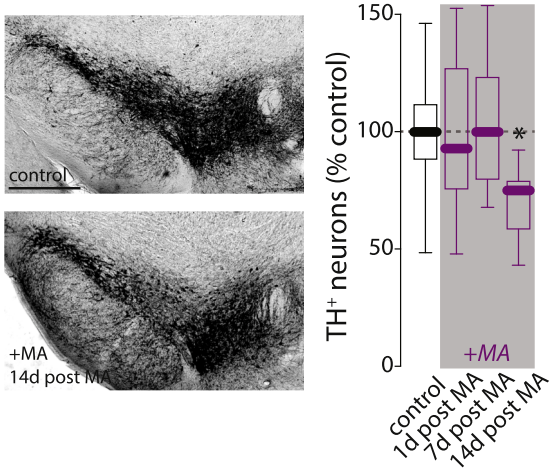

Fig. 2. Subchronic 14-day *in vivo* methamphetamine administration resulted in a delayed loss of substantia nigra pars compacta dopamine neurons. Sample images depicting subchronic 14-day methamphetamine (+MA; 5 mg/kg i.p.)-induced loss of tyrosine hydroxylase expressing (TH^+) neurons (left) in the substantia nigra pars compacta (SNc) 14 days post-MA treatment. Stereological quantification (right) indicates a loss of TH^+ neurons after 14 days (d) but not 1d or 7d post MA treatment; control $n = 10$ mice (median TH^+ cells = 10,215), 1d post MA $n = 10$ mice (median TH^+ cells = 9488), 7d post MA $n = 10$ mice (median TH^+ cells = 10,203), and 14d post MA $n = 10$ mice (median TH^+ cells = 7663); Kruskal-Wallis test with Dunn's *post-hoc*. Scale bars denote 500 μm; $^*p < 0.05$ compared to control.

mitochondrial oxidant stress remained elevated in both axonal and somatic compartments in dopaminergic neurons from MA-treated mice up to two weeks after termination of MA treatment (Fig. 3B & C). In contrast, cytosolic oxidant stress was not significantly affected by treatment at any time point (Fig. 3D, & E) although there does appear to be a trend of increased axonal cytosolic stress possibly suggesting that

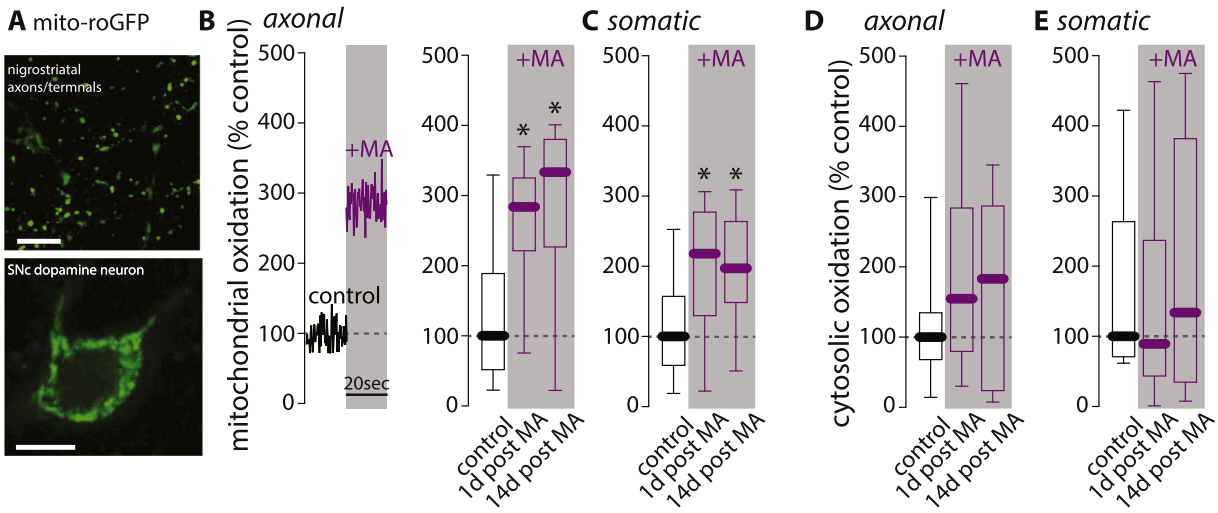

Fig. 3. Subchronic 14-day *in vivo* methamphetamine administration increased axonal and somatic mitochondrial but not cytosolic oxidant stress. A, Sample images depicting the mitochondrially targeted redox biosensor mito-roGFP in nigrostriatal axons in the dorsolateral striatum (top) and cell body (bottom) in the substantia nigra pars compacta (SNc); scale bar denotes 10 μm. B, Sample fluorescent traces (left) depicting differences in axonal mitochondrial oxidant stress expressed as % control between saline treated control and methamphetamine treated (+MA; 14d, 5 mg/kg i.p.) subjects. Quantified data (right) indicate that compared to saline treated controls, +MA increased nigrostriatal axonal mitochondrial oxidant stress when measured after 1 and 14d post MA treatment; Kruskal-Wallis with Dunn's *post-hoc;* control $n = 15$ brain slices/4 mice, 1d post MA $n = 18$ brain slices/4 mice, and 14d post MA $n = 14$ brain slices/4 mice. C, Somatic mitochondrial oxidant stress was also increased in SNc dopamine neurons by +MA after 1d and 14d post MA treatment compared to saline treated controls; Kruskal-Wallis with Dunn's *post-hoc*; control $n = 19$ neurons/7 mice, 1d post MA $n = 21$ neurons/5 mice, and 14d post MA $n = 20$ neurons/6 mice. D, Cytosolic oxidant stress of nigrostriatal axons was unchanged by +MA at 1d or 14d post MA treatment compared to controls; Kruksal-Wallis test; control $n = 11$ brain slices/3 mice, 1d post MA $n = 11$ brain slices/3 mice, and 14d post MA $n = 11$/brain slices/3 mice; $p = 0.3928$. E, Somatic cytosolic oxidant stress of SNc dopamine neurons was also unaffected by +MA at 1d and 14d post MA compared to controls; Kruksal-Wallis test; control $n = 9$ brain slices/2 mice, 1d post MA $n = 21$ brain slices/3 mice, and 14d post MA $n = 11$/brain slices/2 mice; $p = 0.6006$. *$p < 0.05$ compared to control.

cytosolic stress may be elevated in a subset of axons.

Axonal mitochondrial oxidant stress can be elevated by activating MAO (Graves et al., 2020). Although MAO inhibition has no effect on axonal mitochondrial oxidant stress in MA naïve mice (Graves et al., 2020), bath perfusion of the MAO-B inhibitor rasagiline (1 μM) attenuated axonal mitochondrial oxidant stress in *ex vivo* brain slices from MA treated mice (Fig. 4A). This change could have been brought about by dysfunction or downregulation of VMAT2, leading to increased cytosolic DA in MA treated mice. Indeed, reverse transcription of SNc mRNA followed by quantitative polymerase chain reaction (qPCR) analysis of *VMAT2* mRNA abundance revealed that MA treatment for 14 days led to a down-regulation (Fig. 4B).

While the down-regulation of VMAT2 provides an explanation for the elevation in axonal oxidant stress, it doesn't explain why somatic mitochondrial oxidant stress was elevated following MA treatment, as somatic mitochondria are unaffected by MAO-B inhibition (Graves et al., 2020). Previous work has shown that the opening of Cav1 (L-type) Ca^{2+} channels during pacemaking increases somatic mitochondrial oxidant stress in SNc dopaminergic neurons (Guzman et al., 2018; Guzman et al., 2010). Although the Cav1 channel negative allosteric modulator isradipine (5 μM) had no effect on axonal mitochondrial stress in *ex vivo* slices from MA treated mice, it attenuated somatic mitochondrial oxidant stress (Fig. 4C). In contrast, MAO-B inhibition with rasagiline had no effect on MA-induced somatic mitochondrial oxidant stress (Fig. 4C).

There are two simple ways in which MA treatment might have increased Cav1 channel stimulation of mitochondria. One way would be to increase the expression of Cav1 channels, leading to increased influx during pacemaking. *In vitro*, using neuroblastoma derived SH-SY5Y cells, 48 h incubation of a high (50 μM) concentration of MA resulted in an upregulation of Cav1 channels, particularly Cav1.3 channels, which was dependent on D1 DA receptor signaling (Andres et al., 2015). However, our 14 day *in vivo* MA treatment protocol did not change the expression of mRNA coding for the pore-forming subunit of Cav1.3 channels (*CACNAD1)* in the SNc; these channels are the principal drivers of mitochondrial stress in SNc dopaminergic neurons (Fig. 4D) (Guzman et al., 2018). Moreover, quantitative Ca^{2+} imaging using Fura-2 failed to detect any change in somatic cytosolic Ca^{2+} transients in pacemaking SNc dopaminergic neurons in *ex vivo* brain slices from MA-treated mice (Fig. 5A). Another way in which mitochondrial oxidant stress could arise is by increasing the rate of pacemaking, leading to increased bioenergetic demand and stimulation of mitochondrial oxidative phosphorylation; indeed, increasing pacemaking rate elevates mitochondrial oxidant stress in neurons of the dorsal motor nucleus of the vagus (Goldberg et al., 2012). To test this hypothesis, perforated patch recordings (which preserve the intracellular microenvironment) of SNc dopaminergic neurons were made in *ex vivo* brain slices. These recordings revealed a persistent elevation in pacemaking rate after 14 days of MA treatment (Fig. 5B). Thus, the elevation in somatic mitochondrial stress was driven by changes in intrinsic activity and not by changes in Cav1.3 Ca^{2+} channel expression or functional properties.

3.3. Inhibition MAO-B or Cav1 Ca^{2+} channels blunted delayed degeneration

The experiments shown thus far demonstrate that 14 days of MA treatment leads to a persistent elevation in axonal and somatic mitochondrial oxidant stress in SNc dopaminergic neurons. However, the drivers of this stress appear to be regionally specific: in axons, oxidant stress is sensitive to MAO-B inhibition, whereas in the somatodendritic region, stress is sensitive Cav1 Ca^{2+} channels inhibition. To determine whether one or the other of these sources of mitochondrial stress were responsible for the delayed degeneration, mice were first treated for 14 days with MA and then given either the MAO-B inhibitor rasagiline (1 mg/kg/day) or the Cav1 channel negative allosteric modulator isradipine (3 mg/kg/day) for 14 days. At the end of this treatment period, mice were sacrificed and processed for stereological analysis. Surprisingly, inhibition of either MAO-B or Cav1 channels attenuated the loss of

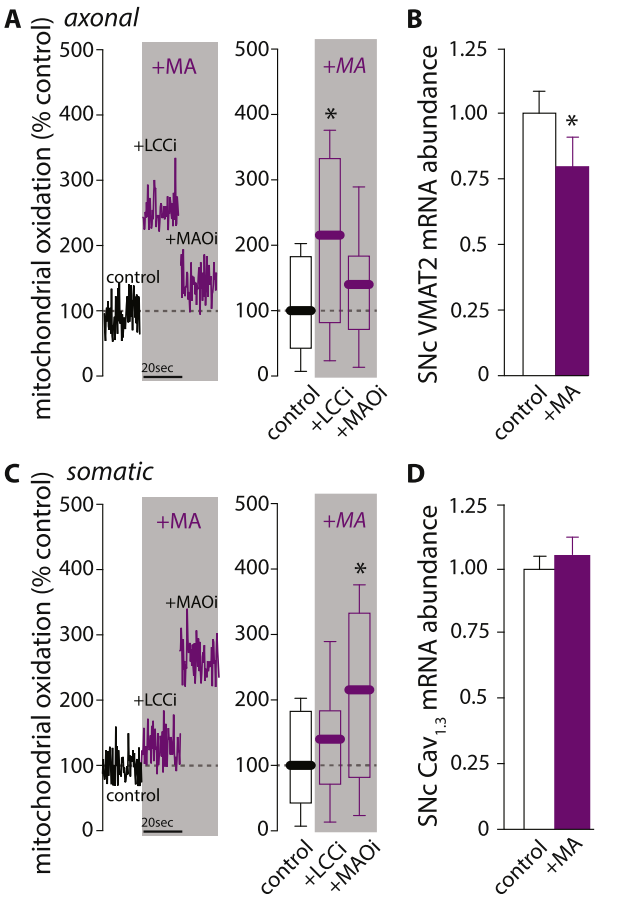

Fig. 4. Elevated Axonal mitochondrial oxidant stress after methamphetamine treatment is MAO-sensitive whereas elevated somatic mitochondrial oxidant stress is L-type Ca^{2+} channel sensitive. A, Sample fluorescent traces (left) depicting differences in axonal mitochondrial oxidant stress expressed as % control between saline treated control and methamphetamine treated (+MA; 14d, 5 mg/kg i.p.; 1d post MA) subjects with aCSF, isradipine (5 μM; +LCCi) or rasagiline (1 μM; +MAOi) bath perfusion in *ex vivo* brain slices. Quantified data (right) indicate that compared to saline treated controls, the +MA-induced increased nigrostriatal axonal mitochondrial oxidant stress was insensitive to +LCCi and was attenuated by +MAOi; Kruskal-Wallis with Dunn's *post-hoc;* control $n = 10$ brain slices/2 mice, +MA + LCCi $n = 13$ brain slices/3 mice, and + MA + MAOi $n = 10$ brain slices/3 mice. B, Mice were treated with saline (control) or MA for 14 days and sacrificed 1 day post MA treatment; tissue entailing the substantia nigra pars compacta (SNc) was dissected for PCR analysis. mRNA encoding the vesicular monoamine transporter 2 (VMAT2) was decreased in mice treated with MA; control $n = 6$ and + MA $n = 5$ mice ($^*p < 0.05$ analyzed using *t*-test). C, Sample fluorescent traces (left) depicting differences in somatic mitochondrial oxidant stress expressed as % control between saline treated control and + MA (14d, 5 mg/kg i.p.; 1d post MA treatment) subjects with aCSF, isradipine (5 μM; +LCCi) or rasagiline (1 μM; +MAOi) bath perfusion in *ex vivo* brain slices. Quantified data (right) indicate that compared to saline treated controls, the +MA-induced increased nigrostriatal somatic mitochondrial oxidant stress was attenuated by +LCCi and was insensitive to +MAOi; Kruskal-Wallis with Dunn's *post-hoc;* control $n = 17$ brain neurons/5 mice, +MA + LCCi $n = 19$ brain neurons/4 mice, and +MA + MAOi n = 11 brain neurons/3 mice. D, mRNA encoding Cav1.3L-type Ca^{2+} channels in the SNc was not changed by +MA; control $n = 6$ and + MA $n = 5$ mice (data analyzed by *t*-test; not significant). $^*p < 0.05$ compared to control.

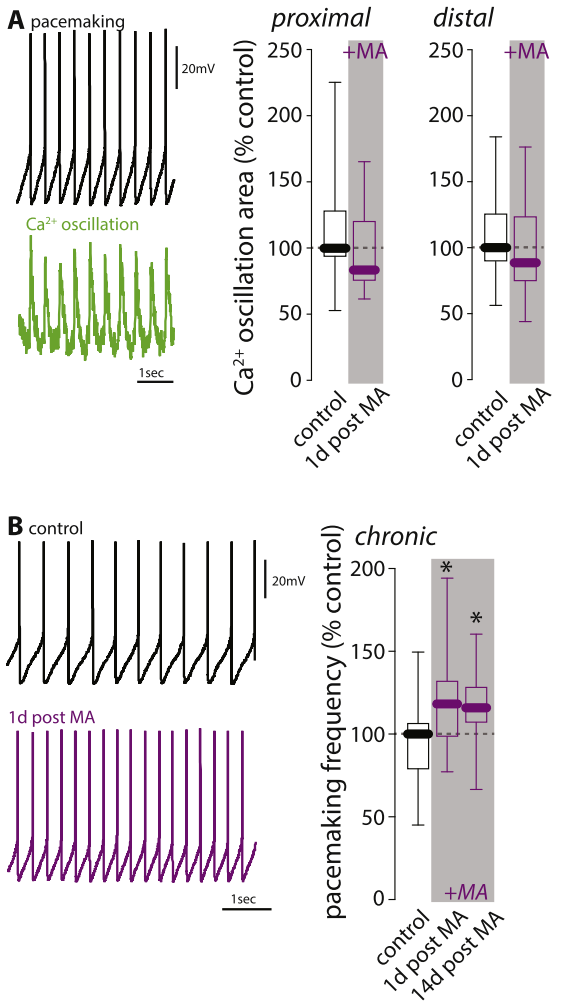

Fig. 5. Subchronic 14-day *in vivo* methamphetamine administration did not alter Ca^{2+} oscillations but accelerated pacemaking activity. A, Mice were treated with methamphetamine for fourteen consecutive days (+MA; 5 mg/kg) and compared to saline treated controls (control); *ex vivo* brain slices were prepared after 1 or 14 days post MA treatment (1d post MA and 14d post MA). Pacemaking associated Ca^{2+} influx was measured using the fluorescent Ca^{2+} indicator Fura-2. Substantia nigra pars compacta dopamine neurons were patched using whole-cell configuration and pacemaking associated Ca^{2+} oscillations in proximal and distal dendrites obtained using two-photon laser scanning microscopy. Sample traces are provided on the left showing pacemaking activity (top) and corresponding Ca^{2+} oscillations measured in a proximal dendrite (bottom). Quantified data (right) show that neither proximal or distal pacemaking associated Ca^{2+} oscillations were changed by +MA; data acquired 1d post MA treatment. Ca^{2+} oscillations were analyzed as oscillation area, normalized to control, and presented as % control. Mann-Whitney non-parametric analyses were used; proximal: control $n = 28$ neurons/5 mice and + MA 1d post $n = 14$ neurons/4 mice; distal: control $n = 28$ neurons/5 mice and 1d post MA $n = 12$ neurons/4 mice. B, Dopaminergic neurons in the substantia nigra pars compacta were recorded from using perforated patch clamp techniques. Sample traces are presented on the left illustrating the difference between control and +MA 1d post MA treatment. Quantified data (right) show that +MA increased the pacemaking frequency when measured 1d and 14d post MA treatment; Kruskal-Wallis with Dunn's *post-hoc*; control $n = 30$ neurons/10 mice, 1d post MA $n = 27$ neurons/9 mice, and 14d post MA $n = 25$ neurons/9 mice. All data was normalized to control group and presented as % control; $^*p < 0.05$ compared to control.

TH^+ SNc dopaminergic neurons (Fig. 6).

4. Discussion

Three conclusions can be drawn from the work presented. First, chronic 28-day (5 mg/kg) MA treatment results in frank SNc dopaminergic degeneration and this degeneration is blocked by concomitant MAO-B inhibition. Second, a shorter 14-day treatment paradigm also results in SNc dopaminergic neuron loss. However, this loss is delayed and does not become apparent until two weeks after the

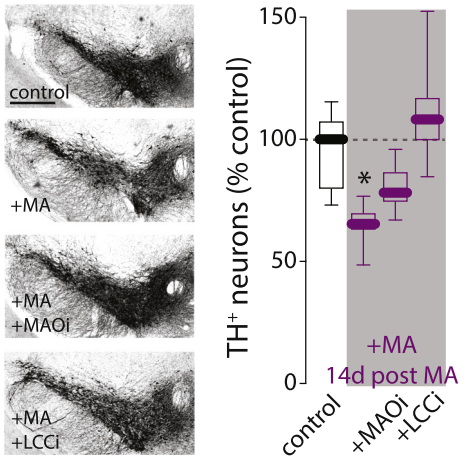

Fig. 6. MAO and L-type Ca^{2+} channel inhibition after methamphetamine treatment is neuroprotective. Sample images depicting subchronic 14-day methamphetamine (+MA; 5 mg/kg i.p.)-induced loss of tyrosine hydroxylase expressing (TH^+) neurons (left) in the substantia nigra pars compacta (SNc) 14d post MA treatment and neuroprotection afforded by treating with the MAO inhibitor rasagiline (+MAOi; 1 mg/kg/day, i.p.) and the L-type Ca^{2+} channel inhibitor isradipine (LCCi; 3 mg/kg/day delivered *via* subcutaneous osmotic minipump). Stereological quantification (right) indicates a loss of TH^+ neurons 14d post MA treatment and this loss was prevented by +MAOi and + LCCi; control $n = 11$ mice (median TH^+ cells $n = 11{,}717$), 14d post MA $n = 9$ mice (median TH^+ cells = 7664), 14d post MA + MAOi $n = 9$ mice (median TH^+ cells $n = 9156$), and 14d post MA + LCCi $n = 7$ mice (median TH^+ cells = 12,683); Kruskal-Wallis test with Dunn's *post-hoc*. Scale bars denote 500 μm; $^*p < 0.05$ compared to control.

cessation of MA treatment. Third, this delayed degeneration is attributable to a combination of axonal and somatic mitochondrial stress, as both remained elevated following cessation of MA treatment and diminishing either attenuated degeneration. The axonal mitochondrial stress appears to stem from deficits in handling of cytosolic DA, as it was accompanied by a down-regulation in VMAT2 and was blocked by inhibition of MAO-B. In contrast, the somatic mitochondrial oxidant stress appears to result from increased pacemaking and concomitant stimulation of mitochondrial oxidative phosphorylation by Ca^{2+} entry through Cav1 (L-type) channels. Taken together, these studies create a new framework for understanding MA toxicity in the brain and point to new therapeutic strategies for lessening the neurological burden of MA abuse.

4.1. Chronic MA administration produced frank SNc dopaminergic degeneration

Most studies of MA toxicity have focused on the consequence of acute binges where subjects are repeatedly administered moderate-to-high doses of MA in a single day. Binge protocols decrease striatal DA, TH, VMAT2, and DAT, some of which may persist for as long as thirty days after cessation of treatment (Ares-Santos et al., 2014; Blaker et al., 2019; Dang et al., 2016; Eyerman and Yamamoto, 2005; Eyerman and Yamamoto, 2007; Frey et al., 1997; Fumagalli et al., 1998; Granado et al., 2010; Granado et al., 2018; Guillot et al., 2008b; Hogan et al., 2000; Hotchkiss and Gibb, 1980; Lohr et al., 2015; Mark et al., 2004; McConnell et al., 2015; Moszczynska and Yamamoto, 2011; Northrop and Yamamoto, 2013; O'Callaghan and Miller, 1994; Reichel et al., 2012; Salvatore et al., 2018; Seiden et al., 1988; Sonsalla et al., 1996; Truong et al., 2005). However, whether these protocols produce frank degeneration is controversial (Ares-Santos et al., 2014; Blaker et al., 2019; Lohr et al., 2015; Sonsalla et al., 1996).

A few studies have examined the consequences of 7–14 day MA administration. These studies report decreased striatal phenotypic markers (DAT, DA concentration), but did not examine neuronal loss (Krasnova et al., 2013; Krasnova et al., 2010; McFadden et al., 2012; Reichel et al., 2012). In our studies, there was a loss of SNc dopaminergic neurons 14 days after completing a 14-day MA treatment regimen or after 28 daily doses of MA. Overt degeneration was confirmed by the loss of a *Gt(ROSA)26Sor* locus reporter that was turned on by Cre recombinase expression under control of the DAT promoter.

Why degeneration was delayed after cessation of the 14-day treatment regimen is unclear. Nevertheless, our results are consistent with previous studies in rats showing that MA self-administration for 14 days produced a similar delayed SNc degeneration (Kousik et al., 2014). In the self-administration paradigm, rats obtained on average 3.7 mg/kg/day MA, which is close to the 5 mg/kg/day used in our protocol. The more rapid appearance of degeneration in our experiments (~14 days) than in the Kousik et al. work (~28 days) may be due to the slightly higher dosing used in our study or to species differences. Whether the MA-induced degenerative changes persist after longer withdrawal periods or whether there is some measure of recovery, remains to be determined.

Another key question is whether MA-induced degeneration preferentially affects one population of dopaminergic neuron or another. SNc dopaminergic neurons differ in many ways (Poulin et al., 2020). In agreement with the possibility of differential vulnerability, binge administration of 3,4-methylenedioxymethamphetamine (MDMA) induces a preferential loss of TH and DAT immunoreactivity in striatal striosomes than the matrix (Granado et al., 2008).

4.2. MA induced neurodegeneration was MAO-dependent

Two processes appear to underlie the delayed SNc dopaminergic loss. One was dependent upon MAO-B, an enzyme that metabolizes cytosolic DA. MA disrupts VMAT2 function resulting in increased concentrations of cytosolic DA (Freyberg et al., 2016; Sulzer et al., 2005). In cell-free systems, DA can both auto-oxidize to generate reactive quinones and when metabolized by MAO generate damaging H_2O_2 and aldehydes (Edmondson, 2014; Goldstein et al., 2013; Sulzer and Zecca, 2000). However, the evidence that either of these events drives neurodegeneration *in vivo* has been indirect. Direct assessment of MA effects on murine and human dopaminergic axon terminals using genetically encoded redox sensors revealed that it increased mitochondrial but not cytosolic stress (Graves et al., 2020). This oxidant stress was traced to elevated DA metabolism by mitochondrially anchored MAO and shuttling of electrons to the electron transport chain, which normally supports the synthesis of ATP needed for synaptic transmission (Graves et al., 2020).

Persistent over-stimulation of MAO by daily MA administration appears, in part, to be responsible for the overt degeneration of dopaminergic neurons, as MAO-B inhibition with rasagiline blunted MA-induced degeneration. Sustained mitochondrial oxidant stress – like that produced by over-stimulation of MAO – is capable of damaging mitochondria and promoting other forms of pathology in dopaminergic neurons (Burbulla et al., 2017; Guzman et al., 2018). MA-induced oxidant stress, coupled with elevated production of reactive aldehydes (Goldstein et al., 2013) may be sufficient to trigger degeneration of axons, which have elevated metabolic stress in the absence of MA (Pissadaki and Bolam, 2013); axonal degeneration would deprive SNc dopaminergic neurons of survival promoting trophic support (Kordower and Burke, 2018). One strategy to sort out the relative contribution mitochondrial oxidant stress and aldehyde production would be to overexpress enzymes that metabolize aldehydes, like ALDH1 (Liu et al., 2014). It is also worth considering the fact that DA is also sequestered and released from dendrites (Rice and Patel, 2015), suggesting that persistent, MA-induced MAO activity could have deleterious effects there too. Indeed, in cultured neurons, dendrites appear to be particularly vulnerable to MA-induced degeneration that has been linked to bioenergetic deficiency (Cubells et al., 1994; Larsen et al., 2002;

Lotharius and O'Malley, 2001).

At first glance, our results appear to be at odds with studies suggesting that MAO inhibition exacerbates MA toxicity (Kuhn et al., 2008; Thomas et al., 2008; Wagner and Walsh, 1991). There are two critical differences between these studies and ours. First, these studies used an acute binge paradigm wherein subjects were administered MA ($\geq$ 5 mg/kg) every 2 h for a total of four injections in one day resulting in a cumulative daily dose more than four times that used in our experiments. Using similar acute binge treatment paradigms, some studies found loss of SNc dopaminergic neurons (Ares-Santos et al., 2014; Sonsalla et al., 1996), while others did not (Blaker et al., 2019; Lohr et al., 2015). In contrast, our study used a chronic protocol with a modest daily MA dose. Second, in 'binge' studies reporting that MAO inhibition exacerbates MA toxicity (Kuhn et al., 2008; Thomas et al., 2008; Wagner and Walsh, 1991), the measure of 'toxicity' was striatal DA content, not neurodegeneration. Striatal DA content is affected by many factors, like DA metabolism, and does not necessarily reflect frank degeneration of dopaminergic neurons. Moreover, more recent work by Thomas and colleagues found no effect of MAO inhibition on striatal DA following MA treatment (Thomas et al., 2009). In addition, our results agree with studies showing that MAO inhibition attenuates 3,4-methylenedioxymethamphetamine (MDMA)-induced decrease in striatal serotonin content (Falk et al., 2002; Sprague and Nichols, 1995). There should be mechanistic parallels between the effects of MAO inhibition on the consequences of MA and MDMA treatment. Thus, not only is the inference that MAO inhibition is toxic in 'binge' MA treatment models questionable, in a treatment paradigm that better mimics the chronic, daily use characteristic of those suffering from a MA use disorder, MAO inhibition clearly blunts degeneration of SNc dopaminergic neurons.

After terminating MA treatment, axonal mitochondrial stress remained elevated and, like the stress induced by acute MA treatment, it was sensitive to MAO-B inhibition, suggesting it was driven by elevated cytosolic DA. Down-regulation of VMAT2 is most likely responsible for this consequence. In agreement with previous work in binge models (Eyerman and Yamamoto, 2007), there was a down-regulation in the expression of the gene coding for VMAT2 after 14 days of MA treatment. Moreover, the MAO-dependent mitochondrial oxidant stress was limited to axons, which are the primary sites of synthesis, packaging and release of DA.

4.3. MA treatment induced a sustained elevation in somatic mitochondrial stress

Chronic MA treatment also elevated somatic mitochondrial stress, but unlike the situation in axons this stress was insensitive to MAO-B inhibition. Elevated somatic stress was accompanied by accelerated pacemaking. Previous work shows that during pacemaking, membrane depolarization opens Cav1.3 Ca^{2+} channels and releases Ca^{2+} from intracellular stores (Guzman et al., 2018; Sanchez-Padilla et al., 2014). This Ca^{2+} signaling drives mitochondrial oxidative phosphorylation and concomitant oxidant stress. Somatic mitochondrial stress has long been linked to the dopaminergic degeneration induced by toxins, like MPTP, rotenone and 6-OHDA (Bove and Perier, 2012; Surmeier et al., 2017b). Indeed, chronic inhibition of Cav1 Ca^{2+} channels by the dihyrdropyridine isradipine attenuated MA-induced degeneration. Several factors might modulate the response to MA. Nrf2 (nuclear factor-erythroid 2-related factor 2) regulates the expression of proteins mediating oxidant defense and knocking it out increases the deleterious consequences of MA binges (Granado et al., 2011). We would predict that down-regulating Nrf2 expression would have the same effect in chronic MA protocols, but this remains to be explored.

What also remains to be determined is why MA treatment caused pacemaking to increase. There are several plausible explanations. One is that MA treatment leads to a disruption in D2 dopamine receptor autoreceptor signaling, effectively removing a 'brake' on pacemaking; this might be accomplished by receptor desensitization (Duda et al., 2016; Sharpe et al., 2014). Another possibility is that the change in pacemaking is being driven by the bioenergetic demand accompanying axonal damage. As both maintenance and repair require energy in the form of ATP and as mitochondria are the principal suppliers of ATP in neurons, MA-induced damage should increase mitochondrial demand. To meet this demand, dopaminergic neurons may increase their pacemaking rate, leading to increased cytosolic Ca^{2+} oscillations and increased stimulation of mitochondrial oxidative phosphorylation (Szibor et al., 2020; Zampese and Surmeier, 2020). However, it also possible that the change is directly related to MAO metabolism of cytosolic DA, hyperpolarization of mitochondria, increased cytosolic Ca^{2+} uptake and decreased activation of Ca^{2+} activated K^+ channels that regulate dopaminergic neuron spiking rate and pattern (Ji and Shepard, 2006). Lastly, it is unclear whether MA treatment and oxidant stress is linked to redox-mediated regulation of perisomatic Kv4 K^+ channels that might influence pacemaking (Subramaniam et al., 2014). Further study is needed to sort these possibilities out.

4.4. MA abuse and PD risk

Epidemiological studies identify a correlation between MA abuse and the risk of developing PD (Callaghan et al., 2010; Callaghan et al., 2012; Curtin et al., 2015). If this linkage is causal, the nature of the connection is uncertain. For more than 30 years, cytosolic DA – which is elevated by MA – has been suspected of being harmful because it can auto-oxidize or generate H_2O_2 (Edmondson, 2014; Sulzer and Zecca, 2000). DA metabolism by MAO also can generate potentially damaging aldehydes (Goldstein et al., 2013). While these processes are undoubtedly engaged in certain circumstances, the question remains as to whether they are engaged *in vivo*. Our recent work found that increasing cytosolic DA, either by levodopa or MA administration, increases mitochondrial, but not cytosolic, oxidant stress (Graves et al., 2020).

5. Conclusions

Mitochondrial oxidant stress is a common feature of many neurodegenerative diseases and the particularly high levels of basal mitochondrial stress in SNc dopaminergic neurons are believed to contribute to their selective vulnerability PD (Pacelli et al., 2015; Surmeier, 2018; Surmeier et al., 2017a). Our results provide a direct, mechanistic linkage between chronic MA abuse, mitochondrial stress and SNc dopaminergic degeneration. Moreover, our studies provide pharmacological strategies that could diminish the damage caused by MA abuse, even after that abuse has taken place.

Author contributions

SMG and DJS designed and directed experiments. SMG, SES, RAT, and YC collected data and SMG and YC analyzed data. SMG and DJS wrote the manuscript and all authors edited the manuscript.

Funding

This work was supported by the JPB Foundation and MJFF (DJS), National Institutes of Health (DA039253, DA051450; SMG), and the Northwestern Memorial Foundation (SMG).

Declaration of Competing Interest

The authors declare no conflict of interest.

Acknowledgements

We thank Sasha Ulrich for technical support.

References

Andres, M.A., et al., 2015. Methamphetamine acutely inhibits voltage-gated calcium channels but chronically up-regulates L-type channels. J. Neurochem. 134, 56–65.

Ares-Santos, S., et al., 2014. Methamphetamine causes degeneration of dopamine cell bodies and terminals of the nigrostriatal pathway evidenced by silver staining. Neuropsychopharmacology. 39, 1066–1080.

Blaker, A.L., et al., 2019. Neurotoxicity to dopamine neurons after the serial exposure to alcohol and methamphetamine: protection by COX-2 antagonism. Brain Behav. Immun. 81, 317–328.

Boileau, I., et al., 2008. Increased vesicular monoamine transporter binding during early abstinence in human methamphetamine users: is VMAT2 a stable dopamine neuron biomarker? J. Neurosci. 28, 9850–9856.

Boileau, I., et al., 2016. Rapid recovery of vesicular dopamine levels in methamphetamine users in early abstinence. Neuropsychopharmacology. 41, 1179–1187.

Bove, J., Perier, C., 2012. Neurotoxin-based models of Parkinson's disease. Neuroscience. 211, 51–76.

Burbulla, L.F., et al., 2017. Dopamine oxidation mediates mitochondrial and lysosomal dysfunction in Parkinson's disease. Science. 357, 1255–1261.

Callaghan, R.C., et al., 2010. Incidence of Parkinson's disease among hospital patients with methamphetamine-use disorders. Mov. Disord. 25, 2333–2339.

Callaghan, R.C., et al., 2012. Increased risk of Parkinson's disease in individuals hospitalized with conditions related to the use of methamphetamine or other amphetamine-type drugs. Drug Alcohol Depend. 120, 35–40.

Cerri, S., et al., 2019. Parkinson's disease in women and men: What's the difference? J. Parkinsons Dis. 9, 501–515.

Chan, C.S., et al., 2007. Rejuvenation' protects neurons in mouse models of Parkinson's disease. Nature. 447, 1081–1086.

Chan, C.S., et al., 2012. Strain-specific regulation of striatal phenotype in Drd2-eGFP BAC transgenic mice. J. Neurosci. 32, 9124–9132.

Cubells, J.F., et al., 1994. Methamphetamine neurotoxicity involves vacuolation of endocytic organelles and dopamine-dependent intracellular oxidative stress. J. Neurosci. 14, 2260–2271.

Curtin, K., et al., 2015. Methamphetamine/amphetamine abuse and risk of Parkinson's disease in Utah: a population-based assessment. Drug Alcohol Depend. 146, 30–38.

Dang, D.K., et al., 2016. Apocynin prevents mitochondrial burdens, microglial activation, and pro-apoptosis induced by a toxic dose of methamphetamine in the striatum of mice via inhibition of p47phox activation by ERK. J. Neuroinflammation 13, 12.

Duda, J., et al., 2016. Converging roles of ion channels, calcium, metabolic stress, and activity pattern of substantia nigra dopaminergic neurons in health and Parkinson's disease. J. Neurochem. 139 (Suppl. 1), 156–178.

Edmondson, D.E., 2014. Hydrogen peroxide produced by mitochondrial monoamine oxidase catalysis: biological implications. Curr. Pharm. Des. 20, 155–160.

Edmondson, D.E., et al., 2009. Molecular and mechanistic properties of the membrane-bound mitochondrial monoamine oxidases. Biochemistry. 48, 4220–4230.

Estep, C.M., et al., 2016. Transient activation of GABAB receptors suppresses SK channel currents in substantia nigra pars compacta dopaminergic neurons. PLoS One 11, e0169044.

Eyerman, D.J., Yamamoto, B.K., 2005. Lobeline attenuates methamphetamine-induced changes in vesicular monoamine transporter 2 immunoreactivity and monoamine depletions in the striatum. J. Pharmacol. Exp. Ther. 312, 160–169.

Eyerman, D.J., Yamamoto, B.K., 2007. A rapid oxidation and persistent decrease in the vesicular monoamine transporter 2 after methamphetamine. J. Neurochem. 103, 1219–1227.

Falk, E.M., et al., 2002. An antisense oligonucleotide targeted at MAO-B attenuates rat striatal serotonergic neurotoxicity induced by MDMA. Pharmacol. Biochem. Behav. 72, 617–622.

Frey, K., et al., 1997. Reduced striatal vesicular monoamine transporters after neurotoxic but not after behaviorally-sensitizing doses of methamphetamine. Eur. J. Pharmacol. 334, 273–279.

Freyberg, Z., et al., 2016. Mechanisms of amphetamine action illuminated through optical monitoring of dopamine synaptic vesicles in Drosophila brain. Nat. Commun. 7, 10652.

Fumagalli, F., et al., 1998. Role of dopamine transporter in methamphetamine-induced neurotoxicity: evidence from mice lacking the transporter. J. Neurosci. 18, 4861–4869.

Fumagalli, F., et al., 1999. Increased methamphetamine neurotoxicity in heterozygous vesicular monoamine transporter 2 knock-out mice. J. Neurosci. 19, 2424–2431.

Galtieri, D.J., et al., 2017. Pedunculopontine glutamatergic neurons control spike patterning in substantia nigra dopaminergic neurons. Elife. 6.

Goldberg, J.A., et al., 2012. Calcium entry induces mitochondrial oxidant stress in vagal neurons at risk in Parkinson's disease. Nat. Neurosci. 15, 1414–1421.

Goldstein, D.S., et al., 2013. Determinants of buildup of the toxic dopamine metabolite DOPAL in Parkinson's disease. J. Neurochem. 126, 591–603.

Granado, N., et al., 2008. Early loss of dopaminergic terminals in striosomes after MDMA administration to mice. Synapse. 62, 80–84.

Granado, N., et al., 2010. Selective vulnerability in striosomes and in the nigrostriatal dopaminergic pathway after methamphetamine administration: early loss of TH in striosomes after methamphetamine. Neurotox. Res. 18, 48–58.

Granado, N., et al., 2011. Nrf2 deficiency potentiates methamphetamine-induced dopaminergic axonal damage and gliosis in the striatum. Glia. 59, 1850–1863.

Granado, N., et al., 2018. Striatal reinnervation process after acute methamphetamine-induced dopaminergic degeneration in mice. Neurotox. Res. 34, 627–639.

Graves, S.M., et al., 2020. Dopamine metabolism by a monoamine oxidase mitochondrial shuttle activates the electron transport chain. Nat. Neurosci. 23, 15–20.

Guillot, T.S., et al., 2008a. PACAP38 increases vesicular monoamine transporter 2 (VMAT2) expression and attenuates methamphetamine toxicity. Neuropeptides. 42, 423–434.

Guillot, T.S., et al., 2008b. Reduced vesicular storage of dopamine exacerbates methamphetamine-induced neurodegeneration and astrogliosis. J. Neurochem. 106, 2205–2217.

Guzman, J.N., et al., 2010. Oxidant stress evoked by pacemaking in dopaminergic neurons is attenuated by DJ-1. Nature. 468, 696–700.

Guzman, J.N., et al., 2018. Systemic isradipine treatment diminishes calcium-dependent mitochondrial oxidant stress. J. Clin. Invest. 128, 2266–2280.

Hogan, K.A., et al., 2000. Analysis of VMAT2 binding after methamphetamine or MPTP treatment: disparity between homogenates and vesicle preparations. J. Neurochem. 74, 2217–2220.

Hotchkiss, A.J., Gibb, J.W., 1980. Long-term effects of multiple doses of methamphetamine on tryptophan hydroxylase and tyrosine hydroxylase activity in rat brain. J. Pharmacol. Exp. Ther. 214, 257–262.

Ilijic, E., et al., 2011. The L-type channel antagonist isradipine is neuroprotective in a mouse model of Parkinson's disease. Neurobiol. Dis. 43, 364–371.

Ji, H., Shepard, P.D., 2006. SK Ca2+-activated K+ channel ligands alter the firing pattern of dopamine-containing neurons in vivo. Neuroscience. 140, 623–633.

Johanson, C.E., et al., 2006. Cognitive function and nigrostriatal markers in abstinent methamphetamine abusers. Psychopharmacology 185, 327–338.

Kish, S.J., et al., 2009. Brain serotonin transporter in human methamphetamine users. Psychopharmacology 202, 649–661.

Kitamura, O., et al., 2007. Immunohistochemical investigation of dopaminergic terminal markers and caspase-3 activation in the striatum of human methamphetamine users. Int. J. Legal Med. 121, 163–168.

Kordower, J.H., Burke, R.E., 2018. Disease modification for Parkinson's disease: axonal regeneration and trophic factors. Mov. Disord. 33, 678–683.

Kousik, S.M., et al., 2014. Methamphetamine self-administration results in persistent dopaminergic pathology: implications for Parkinson's disease risk and reward-seeking. Eur. J. Neurosci. 40, 2707–2714.

Krasnova, I.N., et al., 2010. Methamphetamine self-administration is associated with persistent biochemical alterations in striatal and cortical dopaminergic terminals in the rat. PLoS One 5, e8790.

Krasnova, I.N., et al., 2013. CREB phosphorylation regulates striatal transcriptional responses in the self-administration model of methamphetamine addiction in the rat. Neurobiol. Dis. 58, 132–143.

Kuhn, D.M., et al., 2008. Dopamine disposition in the presynaptic process regulates the severity of methamphetamine-induced neurotoxicity. Ann. N. Y. Acad. Sci. 1139, 118–126.

Larsen, K.E., et al., 2002. Methamphetamine-induced degeneration of dopaminergic neurons involves autophagy and upregulation of dopamine synthesis. J. Neurosci. 22, 8951–8960.

Liu, G., et al., 2014. Aldehyde dehydrogenase 1 defines and protects a nigrostriatal dopaminergic neuron subpopulation. J. Clin. Invest. 124, 3032–3046.

Lohr, K.M., et al., 2015. Increased vesicular monoamine transporter 2 (VMAT2; Slc18a2) protects against methamphetamine toxicity. ACS Chem. Neurosci. 6, 790–799.

Lotharius, J., O'Malley, K.L., 2001. Role of mitochondrial dysfunction and dopamine-dependent oxidative stress in amphetamine-induced toxicity. Ann. Neurol. 49, 79–89.

Mark, K.A., et al., 2004. High-dose methamphetamine acutely activates the striatonigral pathway to increase striatal glutamate and mediate long-term dopamine toxicity. J. Neurosci. 24, 11449–11456.

McCann, U.D., et al., 1998. Reduced striatal dopamine transporter density in abstinent methamphetamine and methcathinone users: evidence from positron emission tomography studies with [11C]WIN-35,428. J. Neurosci. 18, 8417–8422.

McCann, U.D., et al., 2008. Persistent cognitive and dopamine transporter deficits in abstinent methamphetamine users. Synapse. 62, 91–100.

McConnell, S.E., et al., 2015. Characterization of binge-dosed methamphetamine-induced neurotoxicity and neuroinflammation. Neurotoxicology. 50, 131–141.

McFadden, L.M., et al., 2012. Methamphetamine self-administration causes persistent striatal dopaminergic alterations and mitigates the deficits caused by a subsequent methamphetamine exposure. J. Pharmacol. Exp. Ther. 340, 295–303.

Moszczynska, A., Yamamoto, B.K., 2011. Methamphetamine oxidatively damages parkin and decreases the activity of 26S proteasome in vivo. J. Neurochem. 116, 1005–1017.

Moszczynska, A., et al., 2004. Why is parkinsonism not a feature of human methamphetamine users? Brain. 127, 363–370.

Northrop, N.A., Yamamoto, B.K., 2013. Cyclooxygenase activity contributes to the monoaminergic damage caused by serial exposure to stress and methamphetamine. Neuropharmacology. 72, 96–105.

NSDUH, Center for Behavioral Health Statistics and Quality, 2018. 2017 National Survey on Drug Use and Health: Detailed Tables. Substance Abuse and Mental Health Services Administration, Rockville, MD.

O'Callaghan, J.P., Miller, D.B., 1994. Neurotoxicity profiles of substituted amphetamines in the C57BL/6J mouse. J. Pharmacol. Exp. Ther. 270, 741–751.

Pacelli, C., et al., 2015. Elevated mitochondrial bioenergetics and axonal arborization size are key contributors to the vulnerability of dopamine neurons. Curr. Biol. 25, 2349–2360.

Pissadaki, E.K., Bolam, J.P., 2013. The energy cost of action potential propagation in dopamine neurons: clues to susceptibility in Parkinson's disease. Front. Comput. Neurosci. 7, 13.

Poulin, J.F., et al., 2020. Classification of midbrain dopamine neurons using single-cell gene expression profiling approaches. Trends Neurosci. 43, 155–169.

Reichel, C.M., et al., 2012. Methamphetamine-induced changes in the object recognition memory circuit. Neuropharmacology. 62, 1119–1126.
Rice, M.E., Patel, J.C., 2015. Somatodendritic dopamine release: recent mechanistic insights. Philos. Trans. R. Soc. Lond. Ser. B Biol. Sci. 370.
Rumpf, J.J., et al., 2017. Structural abnormality of substantia nigra induced by methamphetamine abuse. Mov. Disord. 32, 1784–1788.
Salvatore, M.F., et al., 2018. Prolonged increase in ser31 tyrosine hydroxylase phosphorylation in substantia nigra following cessation of chronic methamphetamine. Neurotoxicology. 67, 121–128.
Sanchez-Padilla, J., et al., 2014. Mitochondrial oxidant stress in locus coeruleus is regulated by activity and nitric oxide synthase. Nat. Neurosci. 17, 832–840.
Seiden, L.S., et al., 1988. Neurotoxicity in dopamine and 5-hydroxytryptamine terminal fields: a regional analysis in nigrostriatal and mesolimbic projections. Ann. N. Y. Acad. Sci. 537, 161–172.
Sekine, Y., et al., 2001. Methamphetamine-related psychiatric symptoms and reduced brain dopamine transporters studied with PET. Am. J. Psychiatry 158, 1206–1214.
Sekine, Y., et al., 2006. Brain serotonin transporter density and aggression in abstinent methamphetamine abusers. Arch. Gen. Psychiatry 63, 90–100.
Sharpe, A.L., et al., 2014. Methamphetamine self-administration in mice decreases GIRK channel-mediated currents in midbrain dopamine neurons. Int. J. Neuropsychopharmacol. 18.
Sonsalla, P.K., et al., 1996. Treatment of mice with methamphetamine produces cell loss in the substantia nigra. Brain Res. 738, 172–175.
Sprague, J.E., Nichols, D.E., 1995. Inhibition of MAO-B protects against MDMA-induced neurotoxicity in the striatum. Psychopharmacology 118, 357–359.
Subramaniam, M., et al., 2014. Mutant alpha-synuclein enhances firing frequencies in dopamine substantia nigra neurons by oxidative impairment of A-type potassium channels. J. Neurosci. 34, 13586–13599.
Sulzer, D., Zecca, L., 2000. Intraneuronal dopamine-quinone synthesis: a review. Neurotox. Res. 1, 181–195.
Sulzer, D., et al., 2005. Mechanisms of neurotransmitter release by amphetamines: a review. Prog. Neurobiol. 75, 406–433.
Surmeier, D.J., 2018. Determinants of dopaminergic neuron loss in Parkinson's disease. FEBS J. 285, 3657–3668.
Surmeier, D.J., et al., 2017a. Calcium, mitochondrial dysfunction and slowing the progression of Parkinson's disease. Exp. Neurol. 298, 202–209.
Surmeier, D.J., et al., 2017b. Selective neuronal vulnerability in Parkinson disease. Nat. Rev. Neurosci. 18, 101–113.
Szibor, M., et al., 2020. Cytosolic, but not matrix, calcium is essential for adjustment of mitochondrial pyruvate supply. J. Biol. Chem. 295, 4383–4397.
Thomas, D.M., et al., 2008. The newly synthesized pool of dopamine determines the severity of methamphetamine-induced neurotoxicity. J. Neurochem. 105, 605–616.
Thomas, D.M., et al., 2009. Increases in cytoplasmic dopamine compromise the normal resistance of the nucleus accumbens to methamphetamine neurotoxicity. J. Neurochem. 109, 1745–1755.
Todd, G., et al., 2013. Illicit stimulant use is associated with abnormal substantia nigra morphology in humans. PLoS One 8, e56438.
Todd, G., et al., 2016. Adults with a history of illicit amphetamine use exhibit abnormal substantia nigra morphology and parkinsonism. Parkinsonism Relat. Disord. 25, 27–32.
Truong, J.G., et al., 2005. Age-dependent methamphetamine-induced alterations in vesicular monoamine transporter-2 function: implications for neurotoxicity. J. Pharmacol. Exp. Ther. 314, 1087–1092.
Volkow, N.D., et al., 2001a. Loss of dopamine transporters in methamphetamine abusers recovers with protracted abstinence. J. Neurosci. 21, 9414–9418.
Volkow, N.D., et al., 2001b. Association of dopamine transporter reduction with psychomotor impairment in methamphetamine abusers. Am. J. Psychiatry 158, 377–382.
Wagner, G.C., Walsh, S.L., 1991. Evaluation of the effects of inhibition of monoamine oxidase and senescence on methamphetamine-induced neuronal damage. Int. J. Dev. Neurosci. 9, 171–174.
Wilson, J.M., et al., 1996. Striatal dopamine nerve terminal markers in human, chronic methamphetamine users. Nat. Med. 2, 699–703.
Winkelman, T.N.A., et al., 2018. Evaluation of amphetamine-related hospitalizations and associated clinical outcomes and costs in the United States. JAMA Netw. Open 1, e183758.
Zampese, E., Surmeier, D.J., 2020. Calcium, bioenergetics, and Parkinson's disease. Cells. 9.